







Hydraulic traits explain differential responses of Amazonian forests to the 2015 El Niño-induced drought

Fernanda de V. Barros^{1*} , Paulo R. L. Bittencourt^{1,2*}, Mauro Brum^{1*}, Natalia Restrepo-Coupe^{3,4}, Luciano Pereira¹ , Grazielle S. Teodoro⁵ , Scott R. Saleska³, Laura S. Borma⁶, Bradley O. Christoffersen⁷ , Deliane Penha⁸, Luciana F. Alves⁹ , Adriano J. N. Lima¹⁰, Vilany M. C. Carneiro¹⁰, Pierre Gentine¹¹, Jung-Eun Lee¹², Luiz E. O. C. Aragão^{2,13}, Valeriy Ivanov¹⁴, Leila S. M. Leal¹⁵, Alessandro C. Araujo¹⁶ and Rafael S. Oliveira¹ 

¹Department of Plant Biology, Institute of Biology, CP 6109, University of Campinas– UNICAMP, Campinas, SP 13083-970, Brazil; ²College of Life and Environmental Sciences, University of Exeter, Exeter, EX4 4SB, UK; ³Department of Ecology and Evolutionary Biology, University of Arizona, Tucson, AZ 85721, USA; ⁴School of Life Science, University of Technology Sydney, Sydney, NSW 2006, Australia; ⁵Instituto de Ciências Biológicas, Universidade Federal do Pará, Belém, PA 66075-110, Brazil; ⁶Earth System Science Centre, National Institute for Space Research, Av. dos Astronautas, 1.758, São José dos Campos, SP 12227-010, Brazil; ⁷Department of Biology and School of Earth, Environmental and Marine Sciences, University of Texas Rio Grande Valley, Edinburg, TX 78539, USA; ⁸Society, Nature and Development Department, Federal University of Western Pará (UFOPA), Santarém, PA 68035-110, Brazil; ⁹Center for Tropical Research, Institute of the Environment and Sustainability, University of California – Los Angeles, Los Angeles, CA 90095, USA; ¹⁰Laboratório de Manejo Florestal, Instituto Nacional de Pesquisas na Amazônia - INPA, Manaus, AM 69.067-375, Brazil; ¹¹Department of Earth and Environmental Engineering, Columbia University, New York, NY 10027, USA; ¹²Department of Earth and Planetary Sciences, Brown University Providence, 324 Brook Street, Providence, RI 02912, USA; ¹³Remote Sensing Division, National Institute for Space Research, Av. dos Astronautas, 1.758, São José dos Campos, SP 12227-010, Brazil; ¹⁴Department of Civil and Environmental Engineering, University of Michigan, Ann Arbor, MI 48019, USA; ¹⁵Laboratory of Sustainable Systems Analyses, Oriental Amazon Embrapa, Belém, Pará 66083-156, Brazil; ¹⁶LBA Program Micrometeorology Group, INPA, Manaus, Amazonas 69.067-375, Brazil

Summary

Authors for correspondence:

Fernanda de V. Barros

Tel: +55 19 35916177

Email: nandavascon@gmail.com

Paulo R. L. Bittencourt

Tel: +55 19 991331952

Email: paulo09d@gmail.com

Rafael S. Oliveira

Tel: +55 19 988231042

Email: rafaelsoiv@gmail.com

Received: 14 December 2018

Accepted: 28 April 2019

New Phytologist (2019) **223**: 1253–1266

doi: 10.1111/nph.15909

Key words: 2015-ENSO, Amazon tropical forest, drought, embolism resistance, hydraulic traits, plant functional diversity.

Introduction

Increases in the frequency and duration of climatic anomalies, such as drought events induced by the El Niño–Southern Oscillation (ENSO), are resulting in higher plant mortality, including in Amazonia, home of the world's largest contiguous tropical forests (Williamson *et al.*, 2000; Phillips *et al.*, 2010; Lintner

- Reducing uncertainties in the response of tropical forests to global change requires understanding how intra- and interannual climatic variability selects for different species, community functional composition and ecosystem functioning, so that the response to climatic events of differing frequency and severity can be predicted.
- Here we present an extensive dataset of hydraulic traits of dominant species in two tropical Amazon forests with contrasting precipitation regimes – low seasonality forest (LSF) and high seasonality forest (HSF) – and relate them to community and ecosystem response to the El Niño–Southern Oscillation (ENSO) of 2015.
- Hydraulic traits indicated higher drought tolerance in the HSF than in the LSF. Despite more intense drought and lower plant water potentials in HSF during the 2015-ENSO, greater xylem embolism resistance maintained similar hydraulic safety margin as in LSF. This likely explains how ecosystem-scale whole-forest canopy conductance at HSF maintained a similar response to atmospheric drought as at LSF, despite their water transport systems operating at different water potentials.
- Our results indicate that contrasting precipitation regimes (at seasonal and interannual time scales) select for assemblies of hydraulic traits and taxa at the community level, which may have a significant role in modulating forest drought response at ecosystem scales.

et al., 2012; Fu *et al.*, 2013). Amazon forests play a significant role in regional and global carbon and water cycles, and provide essential ecosystem services (Oyama & Nobre, 2003; Malhi *et al.*, 2009; Davidson *et al.*, 2011); many efforts thus seek to understand and predict how these forests respond to drought (Da Costa *et al.*, 2010; Joetzjer *et al.*, 2014; Brienen *et al.*, 2015; Rowland *et al.*, 2015).

Most early ecosystem modelling studies used ‘big leaf’ approaches (in which whole forest responses are modelled after

*These authors contributed equally to this work.

average growth responses of single plants or a small number of plants) that do not represent a diversity of functional strategies; these models tended to predict either large-scale catastrophic forest dieback (Cox *et al.*, 2004; Good *et al.*, 2011) or forest persistence (Friedlingstein *et al.*, 2006; Cox *et al.*, 2013; Huntingford *et al.*, 2013). More recent models which account for diversity in functional growth strategies and landscape heterogeneity tend to simulate more nuanced resilience emerging from trait-based selection among growth strategies (Sakschewski *et al.*, 2016) and more heterogeneous transitions (Levine *et al.*, 2016). The inclusion of functional traits in models is therefore expected to improve simulations of forest drought vulnerability and resilience (Fisher *et al.*, 2015; Gentine *et al.*, 2016; Xu *et al.*, 2016; Konings *et al.*, 2017; Manoli *et al.*, 2018).

Two empirical challenges confront efforts to improve such models: the need to increase knowledge of the composition of relevant functional traits of different systems (Medlyn *et al.*, 2016), and the need to test how such knowledge about functionally different individuals scales to ecosystem behaviour – the scale relevant to interactions with the atmosphere and regional climate. To address these challenges, we investigated two different tropical evergreen forests with contrasting climates and different species compositions by, first, characterizing their differences in terms of functional traits, and then by testing hypotheses for how functional differences would affect whole-ecosystem responses.

For functional diversity, we focus on hydraulic traits, particularly those related to embolism resistance, which are key to explaining such important factors as tree mortality, drought resistance and species distribution (Anderegg *et al.*, 2015, 2016; Rowland *et al.*, 2015; Oliveira *et al.*, 2019). Embolism formation in the xylem decreases water supply to the leaves, forcing plants to reduce transpiration and, consequently, reducing photosynthesis and the energy available for physiological functions (Sperry *et al.*, 2002; McDowell *et al.*, 2008). The water potentials at which plant tissues (i.e. stem xylem) lose 50% or 88% of their conductance (P_{50} or P_{88} , respectively) are common measures of xylem embolism resistance (Tyree & Sperry, 1989; Sperry *et al.*, 2002), while hydraulic safety margins to P_{50} ($HSM_{P_{50}}$) – the difference between the minimum water potential measured in field conditions and P_{50} – is a frequently used index of plant drought resistance (Meinzer *et al.*, 2009). Hydraulic safety margins (e.g. $HSM_{P_{50}}$) are observed in the majority of sampled woody species around the globe to be maintained within a narrow range despite the large diversity of embolism resistance (quantified as P_{50}), which generally increases as mean annual precipitation declines (Choat *et al.*, 2012). Drought resistance is a key strategy affecting the distribution of species along water availability gradients, which act as environmental filters, including or excluding species based on their traits (Engelbrecht *et al.*, 2005, 2007; Markesteijn *et al.*, 2011; Esquivel-Muelbert *et al.*, 2017; Oliveira *et al.*, 2019).

For ecosystem-level behaviour, we focused on whole-forest canopy conductance (G_s), an ecosystem-level trait that is both likely related to the hydraulic traits we are measuring, and which plays a central role in coupling ecosystems to the atmosphere. Critically, canopy conductance includes stomatal conductance (aggregated across all leaves in the canopy), which controls plant

water use and couples the plant water and carbon cycles (Collatz *et al.*, 1991; Lin *et al.*, 2015).

We ask whether different precipitation regimes in different Amazon forests lead to community-scale differences in hydraulic traits, and in vegetation responses to extreme drought events. To address this question, we studied hydraulic traits of dominant tree species in two evergreen tropical forest sites with contrasting rainfall regimes: a low seasonality forest (LSF) characterized by low seasonal and interannual rainfall variability in central Amazon (near Manaus, Brazil), and a high seasonal forest (HSF) with substantial seasonal and interannual precipitation variability in eastern Amazon (near Santarem, Brazil).

We then compared species-, community- and ecosystem-level responses at these two forests during a typical dry season period and during one of the most extreme drought El Niño events (referred to here as 2015-ENSO or just ENSO) ever recorded in Amazon rainforests (Jiménez-Muñoz *et al.*, 2016; Panisset *et al.*, 2018). We hypothesized that:

- 1 More variable precipitation regimes select for more drought-resistant communities. We predict dominant species in the HSF have traits associated with higher drought tolerance than the LSF.
- 2 Communities in environments with higher precipitation variability are less sensitive to extreme drought events than communities in environments with lower precipitation variability. We estimated sensitivity as the change in water potential from a regular year dry season to the 2015-ENSO dry season. We predict that HSF species and the community are less sensitive to the 2015-ENSO than the LSF, and that embolism resistance modulates the magnitude of the response. Additionally, we hypothesize the species response to this El Niño event is mediated by their hydraulic traits.
- 3 Community-level water use responses to atmospheric and soil drought is less intense in forests with more variable precipitation. We predict ecosystem canopy conductance, a measure of plant community water use response to environment changes, is less sensitive to vapour pressure deficit and cumulative water deficit in HSF than in LSF.

To test these hypotheses, we combine a unique dataset of xylem embolism resistance, plant water potential (i.e. the physical driver of embolism formation) and canopy conductance in tropical forest species, in the novel context of a strong El Niño event. We propose an approach that allows us to scale species-level hydraulic traits to community-level properties, contributing to the critical overarching goal of linking individual plant trait composition to ecosystem level functioning.

Materials and Methods

Study sites

This study was carried out at two Large-Scale Biosphere–Atmosphere Experiment in Amazon forest (LBA) sites, with contrasting precipitation regimes. The low seasonality forest (LSF) is located in central Amazonia, at the Cuieras Biological Reserve (K34 site), near Manaus, Amazonas, Brazil (60°21'W, 2°61'S). The mean annual precipitation is *c.* 2400 mm, with 2 months of

dry season (precipitation < 100 mm) in July and August (Araujo *et al.*, 2002; De Gonçalves *et al.*, 2013). The higher seasonality forest (HSF) is located in the eastern Amazonia in the Tapajós National Forest (K67 site), near Santarém, Pará, Brazil (54°58'W, 2°51'S). It is drier than the Manaus region, with an annual mean precipitation of *c.* 1900 mm (Parrotta *et al.*, 1995), a longer dry season (5 months, on average) and higher interannual climatic variability. Average annual vapour pressure deficit (VPD) at the HSF site is slightly higher than at LSF (means \pm SD of 0.94 ± 0.3 kPa and 0.84 ± 0.34 kPa, respectively), however dry season VPDs do not differ between the sites (1.05 ± 0.18 kPa and 1.08 ± 0.26 kPa, for the HSF and LSF, respectively; Supporting Information Fig. S1). The LSF soils are characterized by tertiary sediments covered by clayey Oxisols on the plateaus and sandy Spodosols on the valley bottoms (Araujo *et al.*, 2002), whereas the HSF soils are clayey Oxisols, deeply weathered, with no concretions or impeding layers, at least in the upper 12 m (Oliveira *et al.*, 2005; Nepstad *et al.*, 2007).

Species selection

At each site, we selected locally and regionally abundant woody species or genera that contribute significantly to Amazon forest biomass (Ter Steege *et al.*, 2013; Fauset *et al.*, 2015). We studied 17 species in the LSF and nine in the HSF (Table S1; see Brum *et al.*, 2018), which correspond, respectively, to 13.7% and 35.0% of the total forest stem basal area. Embolism vulnerability curves were also measured for three additional species in the HSF (*Manilkara huberi*, *Tachigali chrysophylla* and *Minquartia guianensis*, representing 6.70%, 3.94% and 0.07% of total forest stem basal area).

The LSF and HSF sites differ in species richness, but mainly in terms of dominance homogeneity (Carneiro, 2004; Vieira *et al.*, 2004; Longo, 2013), which led us to sample more species in the LSF to reach a minimum of 10% of forest stem basal area (Table S1). According to previous surveys, which used trees with stem diameter at breast height (DBH) > 10 cm, the species density at the LSF is *c.* 153.2 species ha⁻¹ (based on 3.5-ha sampling, measured on the plateaus with total basal area of 28.3 m² ha⁻¹, Carneiro, 2004), while at the HSF the density was 133 species ha⁻¹ (4-ha transects sampling, Vieira *et al.*, 2004; with total basal area of 30.8 m² ha⁻¹, Pyle *et al.*, 2008 updated by Longo, 2013). The dominance in the LSF is more homogeneous, and the most dominant tree species (i.e. *Eschweilera wachenheimii*) represents 3.02% of total basal area, followed by a few species between 1% and 2% (Carneiro, 2004); whereas in the HSF, few species are locally hyperdominant (i.e. *Erisma uncinatum*, *Chamaecrista xinguensis* and *Coussarea albescens*, corresponding to 11.1%, 6.1% and 4.6% of the total basal area, respectively).

Hydraulic traits

Xylem vulnerability to embolism was assessed by the relationship between the percentage loss of xylem conductivity (PLC) and xylem water potential (Ψ). PLC was estimated from percentage air discharge (PAD) using the pneumatic method (Pereira *et al.*,

2016). To obtain these curves, we collected sun-exposed branches longer than 1 m in length early in the morning, from one to three individuals per tree species (Table S1) with DBH across species ranging from 2.7 to 98.0 cm. For some species, we sampled only one individual due to difficulties of access to very tall trees (e.g. > 35 m height). We cut a branch under water inside a bucket and covered it with a plastic bag overnight before measurements (following Oliveira *et al.*, 2019 and Brum *et al.*, 2018). To induce cavitation, we used the bench dehydration method (Sperry *et al.*, 1988). Stem Ψ was measured as leaf Ψ after equilibrating the branch inside a black plastic bag for at least 1 h before making the measurement. We measured leaf Ψ (MPa) with a pressure chamber (PMS 1000; PMS Instruments Co., Albany, OR, USA). We calculated P₅₀ and P₈₈, defined as the water potentials at which the tissue loses 50% and 88% of its hydraulic conductivity, respectively, by fitting a sigmoidal function to the data (Pammenter & Vander Willigen, 1998):

$$\text{PAD} = \frac{100}{1 + \exp\left(\frac{S_p}{25} (\Psi_x - \Psi_{p50})\right)}$$

where PAD (percentage of air discharge) and Ψ_x (xylem water potential, MPa) are the measurement data, to which the parameters Ψ_{p50} (xylem water potential, when PAD equals 50%) and S_p (slope of the curve, % PAD MPa⁻¹) were fitted.

The minimum leaf water potential (Ψ_{\min}) was measured during the peak of the dry season of an ENSO (Ψ_{ENSO}) and non-ENSO (Ψ_{nonENSO}) year. The Ψ_{nonENSO} was measured during the dry season in August 2016 and December 2014, for the LSF and HSF sites, respectively. The Ψ_{ENSO} was measured during the driest period of the ENSO event in October 2015 for the LSF and December 2015 for the HSF. The driest interval was determined from the cumulative water deficits for both sites (Fig. 1) (CMWD; see Microclimatic and soil data below). The leaf Ψ was measured with a pressure chamber in two or three leaves of the same individuals used to measure the vulnerability curves. Leaves were collected between 12:00 and 14:30 h from sun-exposed branches. For both sites, the water potential was collected over an interval of < 7 d in each period (ENSO or non-ENSO). There were a few short and light rain events in the LSF during this sampling period, however they were insufficient to increase soil moisture. The water potential was always measured after at least 1 day without rain. In the HSF there was no rain during the months during which Ψ was measured.

Species hydraulic safety margins (HSM) with respect to P₅₀ and P₈₈ (HSM_{P50} and HSM_{P88}, respectively) were calculated as minimum leaf Ψ (Ψ_{nonENSO} and Ψ_{ENSO}) minus P₅₀, or P₈₈, respectively. The HSM of the non-ENSO period is thus referred to as HSM_{nonENSO} and that of the ENSO period, as HSM_{ENSO}. We assumed that leaf Ψ was a suitable estimator of xylem Ψ in terminal branches.

Wood anatomy

We collected wood samples from 2nd or 3rd order branches (diameter from *c.* 1 to 2 cm, i.e. the same as used for vulnerability curves) for

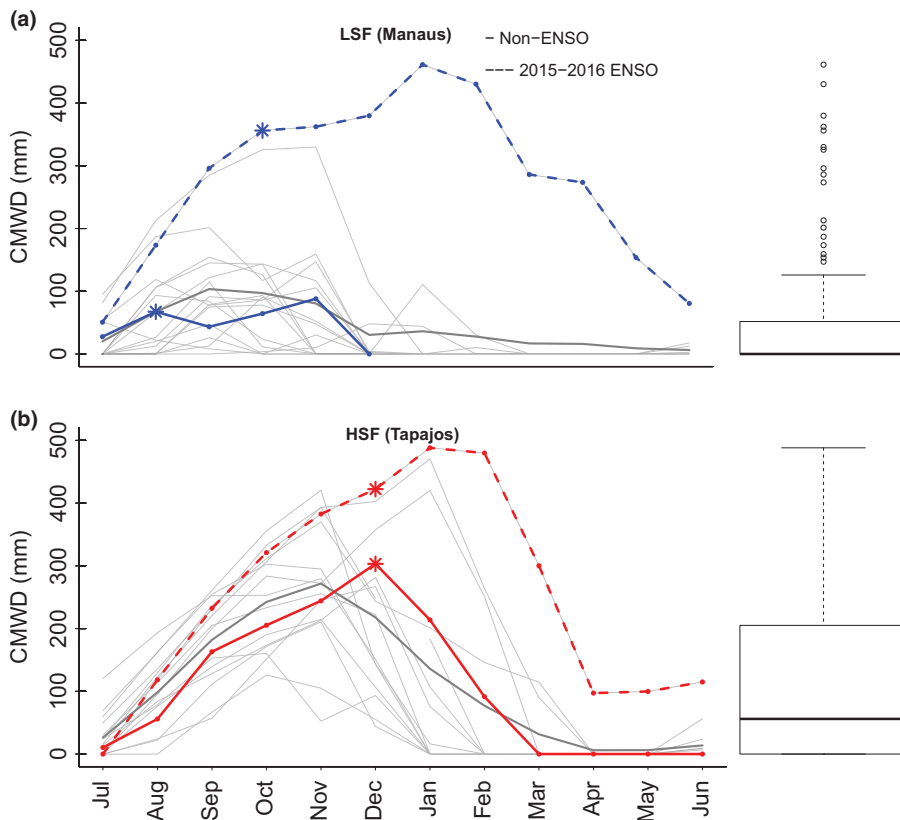


Fig. 1 Monthly cumulative water deficit (mm) from 1999 to 2016 for Manaus (a), and Tapajós (b). Blue and red lines correspond to the periods of water potential measurements at each site for LSF (low seasonal forest; Manaus) and HSF (high seasonal forest; Tapajós), respectively: the solid line represents the non-ENSO year (2014–2015 for Tapajós and 2016–2017 for Manaus), and the dashed line the 2015–2016 ENSO year. Grey lines represent all other years and the thick grey line is the mean across all years, including the ENSO year. Asterisks on blue and red lines denote the months during which the water potential data were collected. Boxplot inserts represent CMWD distribution for each site. Whiskers are either maximum/minimum value or, when outliers are present, 1.5 interquartile range above/below the quartiles 2 and 3.

anatomy. We kept the samples in formalin-acetic acid-alcohol (FAA) for a few days and then exchanged this for 50% alcohol to maintain the wood tissue integrity. We cut the samples using a manual microtome, dyed them with safranin and toluidine blue, and placed them on microscope slides. For each individual sample, we took photographs from three regions of different xylem slices (three per individual) using a digital camera (DP71; Olympus Corp., Tokyo, Japan) coupled to a polarizing microscope (Olympus BX51). The images were processed using IMAGE J software (v.1.6.0_20) (Schneider *et al.*, 2012). For each image, we measured the area of each vessel, the total vessel area (VA; mm² of vessel area per mm² of xylem area) and their density (VD; number of vessels per mm² of xylem area). We calculated effective vessel diameters from the area, assuming vessels were circular. From these data we calculated the vessel hydraulic diameter (D_h ; μm) and the theoretical specific hydraulic conductance of the xylem (K_h ; kg MPa⁻¹ s⁻¹ m⁻³) using the Poiseuille Law (Scholz *et al.*, 2013) as:

$$D_h = \left(\sum_1^n D_i^4 \right)^{\frac{1}{4}}$$

$$K_h = \left(\frac{\pi \rho}{128 \eta A} \right) \sum_1^n D_i^4$$

where D_i is each individual vessel diameter from 1 to n in the photographed xylem area A ; π is pi; ρ and η are the density of water (996.7867 kg m⁻³) and water dynamic viscosity (8.9 $\times 10^{-4}$ Pa s) at 26°C, respectively.

Dominance-weighted traits

We used the species relative dominance (percentage stem basal area of each species in each forest) to calculate the dominance-weighted mean (DWM) for each hydraulic trait, which we use as an estimate of the community-weighted mean (CWM; Garnier *et al.*, 2004). The DWM was calculated from a subsample of the species in each community once, as to achieve 50% of the hyper-diverse LSF dominance, it would require sampling at least 53 species. Our rationale relies on the fact that the DWM from a subsample of species in the community is valid as long as: (1) no single species and trait value exerts stronger influence over the CWM value; or (2) sample weight and sample value are independent, and the estimated weighted mean of a subsample of the data should approximate the true weighted mean (see Methods S1).

For both LSF and HSF we did not detect any relationship between the trait value and the species dominance, and the most dominant species were not outliers. Furthermore, to evaluate whether our results have biases due to the low coverage of basal area of the LSF, we carried out additional analyses to demonstrate that there was no change in the estimates when a larger data sample is considered. Since the contribution to the basal area is homogeneously distributed across many species and the traits are assumed to vary randomly, this enables us to assume the DWM as a good estimator of the CWM and scale results to the whole community. Additionally, we used the biogeographic dry-affiliation index as a trait of the genera in each site (Esquivel-Muelbert *et al.*, 2017, 2018; Methods S2) to evaluate the community

functional composition, that is, the dry affiliation of the whole community at each site.

Microclimatic and soil data

We measured meteorological conditions at both eddy flux tower sites (1999 to 2016; update from Restrepo-Coupe *et al.*, 2016; details in Methods S3). For each location we used the cumulative monthly water deficit (CMWD; mm) as a measure of soil water deficit, calculated as in Aragão *et al.* (2007), except that we used a positive sign to denote convention for the deficit. CMWD was calculated for each month as the cumulative excess of evapotranspiration less precipitation, starting in the wet season of 1999 for LSF, and 2002 for the HSF: ()

$$\text{CMWD}_m = \text{CMWD}_{m-1} + \text{ET}_m - P_m$$

where ET_m is monthly evapotranspiration (mm), P_m is monthly precipitation (mm) and CMWD_m is the cumulative water deficit for month m (mm) and CMWD_{m-1} is that for the previous month. CMWD_m was initialized at zero for the first month and was reset to zero whenever it became negative (i.e. there was a water surplus and not a deficit). The annual mean CMWD was 43.6 ± 47.3 for the LSF, and 109.1 ± 49.4 for the HSF, while the mean annual peak of CMWD was 154.8 ± 118.6 mm for LSF, and 333.1 ± 110.8 mm for the HSF (Fig. 1).

To verify that the estimated CMWD was a good proxy for the more physiologically relevant soil moisture deficit, we assessed the correlation of CMWD with monthly averaged soil volumetric water content (SWC) measurements ($\text{cm}^3 \text{cm}^{-3}$) available at each site. The SWC was measured hourly from October 2015 to August 2016 at the LSF (depths of 0.8, 1.6, 2.4 m; L. Borma *et al.*, unpublished data) and from August 2008 to March 2017 (with a 4-yr gap from 2012 to 2015) at the HSF (depths of 0.1, 1.0, 2.0 m; B. Christoffersen *et al.*, unpublished data). We obtained soil water retention curves for LSF from L. Borma *et al.* (unpublished). Using the time series that overlaps between the two sites (2015 and 2016), the monthly CMWD explained 46% ($F_{(1,9)} = 7.57$; $P = 0.02$ for LSF) and 65% ($F_{(1,52)} = 95.49$; $P < 0.001$ for HSF) of the variation in the soil water content (0 to 2.0–2.4 m soil depth) (Fig. S2), confirming that CMWD could be used as a suitable proxy for soil water deficit.

Canopy conductance

To obtain the ecosystem canopy conductance (G_s ; mm s^{-1}) we used eddy covariance data from both sites (LBA data from 2002 to 2016, see Methods S3). We calculated G_s through the inversion of the Penman–Monteith (PM) equation (Methods S4). We restricted estimates of G_s to times when the canopy was dry (all data up to 12 h after precipitation were removed), so we could justifiably assume that most of the flux was due to transpiration. Eddy covariance, microclimatic and soil data are available at LBA

data repository (LBA DIS; see https://daac.ornl.gov/cgi-bin/data_set_lister.pl?p=11).

Data analysis

To address our first hypothesis, whether traits from LSF species had less drought-resistant traits than HSF species, we used a one-tailed statistical Welch's t -test, and to evaluate the differences in dominance-weighted means we used a Monte Carlo approach with the difference in weighted mean as the test statistic, randomizing the site and repeating 10 000 times.

To evaluate our second hypothesis, whether the dry season leaf water potential (Ψ_{\min}) of the species was affected by the 2015-ENSO in relation to a non-ENSO year and whether the effect differed between sites, we used a general mixed model with species as random factor affecting intercept to account for the same species being measured in the ENSO and non-ENSO year in each site. This has a similar effect of pairing the species in a paired t -test. Additionally, to better understand ENSO effects, we evaluated whether Ψ_{\min} variation could also be accounted by the atmospheric and soil water deficits (monthly maximum VPD and monthly CMWD) when the Ψ_{\min} was measured. To evaluate if the species response to ENSO was modulated by hydraulic traits, we tested whether the difference in species Ψ_{\min} from ENSO to non-ENSO year ($\Delta\Psi$) was related to hydraulic traits using general fixed effects model.

For the third hypothesis, we evaluated whether effects of VPD and CMWD, measures of atmospheric and soil water stress, on G_s differed between HSF and LSF. As periods of soil drought usually occur with atmospheric drought, we had to first remove the correlation between VPD and CMWD. For this we modelled $\text{VPD} \sim \text{CMWD}$ and site to obtain a VPD independent from the CMWD measure (VPD_r for VPD residuals). In the same way, we modelled $\text{CMWD} \sim \text{VPD}$ and site to obtain a CMWD independent from VPD (CMWD_r). With independent VPD and CMWD measures, we tested whether G_s had a fixed VPD_r and CMWD_r effect and whether site (HSF and LSF) had an additive or interactive effect on G_s . For the above analysis and for obtaining CMWD_r and VPD_r , we used general mixed effect models, with month of the year as random factor affecting slope, to control for temporal autocorrelation of variables. The same analyses were performed to evapotranspiration (ET). Finally, to evaluate whether the ecosystem-level water use (G_s) was modulated by hydraulic traits, we analysed if dominance-weighted P_{50} and hydraulic safety margin affected G_s .

Part of the difficulty in analysing atmospheric and soil drought effects is that both are usually correlated (i.e. rainless periods usually have drier atmosphere). To remove this correlation from our dataset, we used only data with CMWD higher than 0, and observations from July to December of 2015. This approach was justified as our goal is to evaluate drought response of G_s , and the data from January to June is usually rainy (precipitation > 100 mm month $^{-1}$). Moreover, LSF had almost no data with $\text{CMWD} > 0$ mm in this wet period, and it would only carry information about G_s response to VPD in wet conditions. For all statistical analyses, data processing and curve fitting, we used R

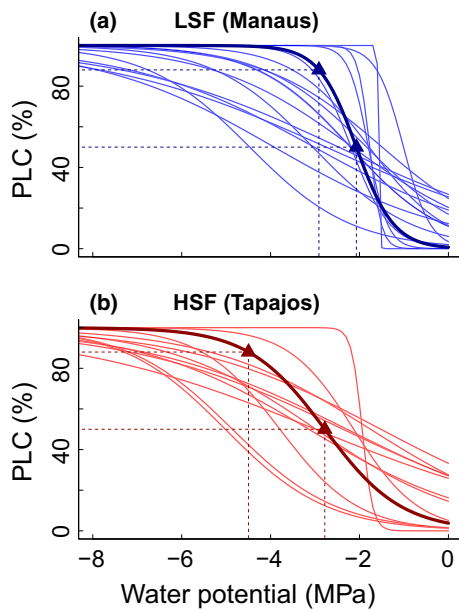


Fig. 2 Hydraulic vulnerability curves for different species at (a) LSF (low seasonal forest) and (b) HSF (high seasonal forest). The thicker lines denote the dominance-weighted vulnerability curve for each forest (blue for LSF and red for HSF).

(R Core Team, 2018, v.3.5), and further information about the analysis functions and packages can be found in the Supporting Information Methods S5.

Results

Hydraulic trait differences between the two forests

The LSF had less embolism-resistant hydraulic vulnerability curves than HSF due to higher P_{88} (-4.08 ± 1.83 MPa vs -5.33 ± 1.49 MPa, $P=0.027$; Fig. 2), and a marginally significant difference in P_{50} between the two forests (-2.34 ± 0.89 MPa and -2.90 ± 1.15 MPa, respectively, $P=0.085$; Figs 2, 3a; see Tables S1 and S2 for results summary). Different P_{88} , even if the P_{50} was similar, is only possible if HSF has a shallower slope than LSF species hydraulic vulnerability curves, consistent with our observations of a marginally significant difference in slopes (Fig. 2; slope difference $P=0.07$; Table S2). Corroborating these results, the dry-affiliation index (represented by the probability of recording a higher dry-affiliated precipitation centre of gravity value than that observed by chance) revealed differences in the HSF and LSF community functional composition (details in Methods S2). We found a dominance of dry-affiliated taxa for HSF compared to LSF (0.73 ± 0.4 for HSF and 0.86 ± 0.3 for LSF; $t=4.8$, $df=339.9$, $P<0.001$) (Fig. 4).

The minimum water potential in the non-ENSO year (Ψ_{nonENSO}) was higher ($P<0.01$) in the LSF (-1.09 ± 0.43 MPa) than in HSF (-1.88 ± 0.58 MPa), however the hydraulic safety margins (i.e. non-ENSO $\text{HSM}_{P_{50}}$ and $\text{HSM}_{P_{88}}$) did not differ between the two forests ($P=0.38$ and $P=0.23$) (Fig. 3c–e; Table S2). The xylem anatomy of the HSF and LSF species also showed significant differences for all

inspected traits: vessel density, vessel area, potential specific hydraulic conductance and hydraulic diameter (Fig. 3f–i; Table S2). Xylem vessel area was higher at the LSF site than at the HSF site ($P=0.03$), and so were the hydraulic diameter ($P=0.04$) and the potential specific conductance ($P=0.04$; Fig. 3, Table S2), while the vessel density was 71% higher at HSF ($P=0.01$; Fig. 3f; Table S2).

The analysis comparing the dominance-weighted mean of LSF and HSF showed similar patterns, with P_{88} of HSF forest being lower than LSF, and P_{50} and slope marginally different (see Table S2). However, this analysis did not detect differences in anatomical traits, possible because of the lower statistical power of the test and the high value of the 95% confidence intervals of the mean for those traits.

Species- and community-level responses to the 2015-ENSO-induced drought

The 2015-ENSO climatic effects were observed in both forests, as the CMWD reached values higher than historical means of the driest months recorded since 1998 (Fig. 1). The 2015-ENSO-induced CMWD was largest in the HSF, but absolute and relative changes from the 1998–2014 average of annual maximum CMWD were higher in LSF, with an increase of 306.4 mm (197%; 154.8–461.2 mm) vs 155 mm (46%; 333.1–488.1 mm) in HSF. The Ψ_{nonENSO} and Ψ_{ENSO} measurements at the LSF site were performed during a CMWD of 67.4 mm, and 356.1 mm, respectively; whereas in the HSF, Ψ_{nonENSO} and Ψ_{ENSO} were measured when the CMWD reached 303.2 mm and 422.3 mm, respectively (Figs 1, 5a), confirming the different CMWD conditions when the Ψ_{min} was measured in both forests.

At both LSF and HSF sites, Ψ_{min} was significantly reduced during the ENSO period ($P<0.001$; see Table S3 for statistical summaries), although the effect of ENSO on Ψ_{min} was not very large (0.6 and 0.5 MPa drop for LSF and HSF, respectively). Site had an additive effect on Ψ_{min} ($P=0.006$), with the HSF Ψ_{min} being on average -0.72 MPa lower than LSF (Fig. 5a), but there was no interaction between site and ENSO ($P=0.12$), indicating the 2015-ENSO effect on Ψ_{min} was similar in both areas. The model explained 68% of Ψ_{min} variability, where ENSO and site explained 32% (conditional and marginal R^2 , respectively).

At the species level, responses to the 2015-ENSO event were heterogeneous (Fig. 5b,c). At the LSF site, Ψ_{min} declined in almost all species during ENSO, while at HSF the responses were more diverse, with a majority of species (*Miconia* sp., *C. albescens*, *E. uchi* and *R. pubiflora*, *M. itauba*) showing a steep drop in Ψ_{min} , while a minority (four of nine) showed no detectable change (the slight increases seen in Fig 5 are in the range of the measurement error).

Monthly maximum VPD was related to Ψ_{min} ($P<0.001$; Fig. 5c, Table S3) but only with a significant site interactive ($P=0.008$) and additive ($P=0.001$) effect on VPD. CMWD was related to Ψ_{min} ($P<0.001$; Fig. 4b; Table S3) but site had no interactive or additive effect on Ψ_{min} ($P=0.31$ and $P=0.11$). The CMWD and VPD of this dataset were related ($r=0.56$) as the month with higher VPD also had higher CMWD, which

precludes us from inferring whether the VPD or CMWD effect is dominating the Ψ_{\min} variability. However, VPD requiring additional explanation of site to explain Ψ_{\min} suggests that CMWD contains additional information not contained in VPD, possibly the correlation with site, which absorbed the site effect on Ψ_{\min} , making CMWD the only significant effect in the model. This effect can be seen in Fig. 5(b,c).

The leaf water potential change, comparing non-ENSO to 2015-ENSO ($\Delta\Psi$), was related to embolism resistance for both P_{50} and P_{88} ($P=0.017$; $r^2=0.21$ and $P=0.019$; $r^2=0.21$, respectively; Fig. 6). Species with higher embolism resistance had higher changes in $\Delta\Psi$. Site effects on P_{50} and P_{88} were not significant for additive effect ($P=0.77$ and $P=0.32$) or interaction effect ($P=0.15$ and $P=0.13$), indicating $\Delta\Psi$ is similarly modulated by embolism resistance in both sites. Anatomical traits were not related to $\Delta\Psi$ ($P>0.20$ for all anatomical traits). P_{50} and P_{88} had the same explanatory power of $\Delta\Psi$ ($r^2=0.21$), likely due to both being strongly correlated ($r=0.74$).

Ecosystem-level functional responses to drought

Both CMWD and VPD from July to December were highly correlated ($r=0.41$), particularly for HSF ($r=0.53$). This correlation was removed using the residuals of one variable modelled with the other as predictor and site as additive factor (Table S4). The residuals of VPD (VPD_r) did not carry any more signal of CMWD for both sites ($r<0.01$), and the residuals of CMWD ($CMWD_r$) did not carry any VPD signal ($r=-0.07$).

Canopy conductance (G_s) was significantly affected by VPD_r ($P<0.001$; $R^2=0.40$), with no additive or interactive site effect, while $CMWD_r$ was unrelated to G_s ($P=0.10$; Fig. S3; Table S4). Given the lack of evidence for a VPD-independent signal of CMWD on G_s , we remodelled G_s as a function of VPD (Fig. 7). We found each unit of VPD caused a decreased in G_s of 5.1 mm s^{-1} ($P<0.001$) and VPD explained 40% of G_s variability. Site had no significant additive or interactive influence on G_s ($P=0.91$ and $P=0.08$), indicating HSF and LSF respond

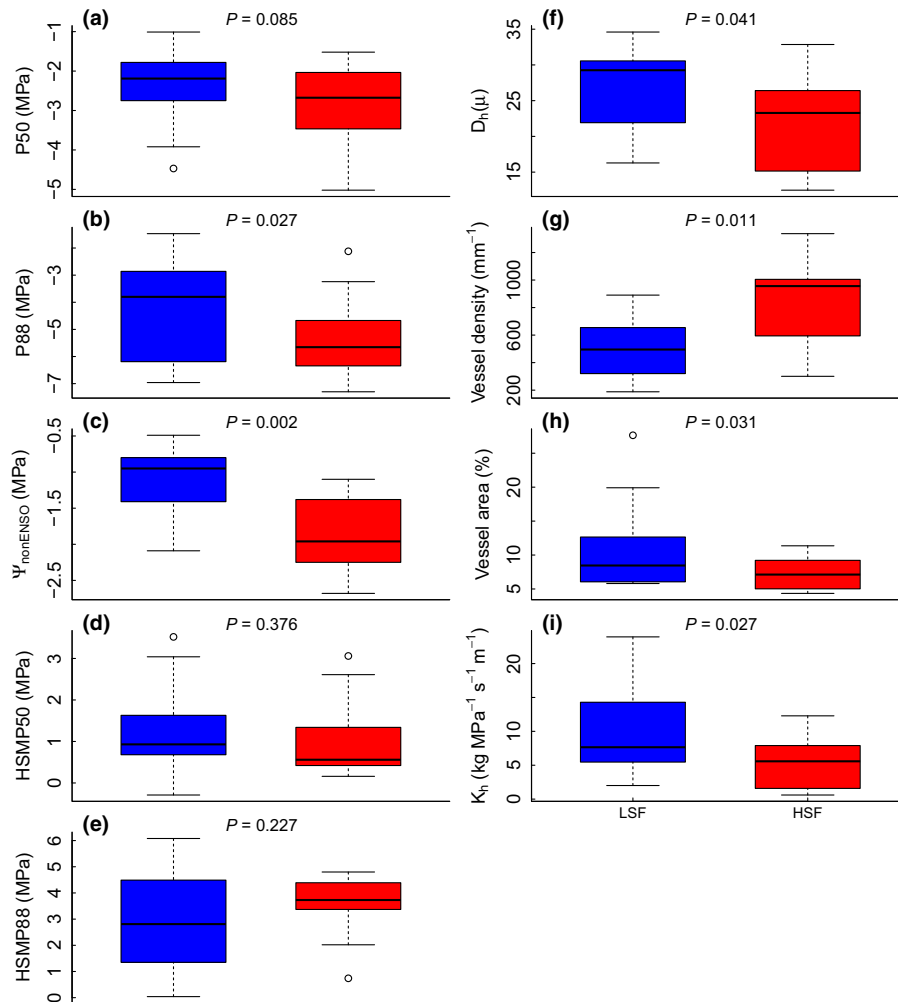


Fig. 3 Hydraulic and anatomical trait distributions for LSF (blue) and HSF (red): (a) P_{50} (MPa); (b) P_{88} (MPa); (c) minimum midday (12:00–14:30 h) water potential for the non-ENSO year (MPa); (d) P_{50} hydraulic safety margin for the non-ENSO year (MPa); (e) P_{88} hydraulic safety margin for the non-ENSO year (MPa); (f) D_v – Hydraulic diameter (mm), (g) Vessel density (vessels mm^{-2}); (h) Vessel area (% vessel area per xylem area); and (i) Potential specific conductance (K_t ; $\text{kg MPa}^{-1} \text{ s}^{-1} \text{ m}^{-1}$). Whiskers are either maximum/minimum value or, when outliers are present, 1.5 interquartile range above/below the quartiles 2 and 3.

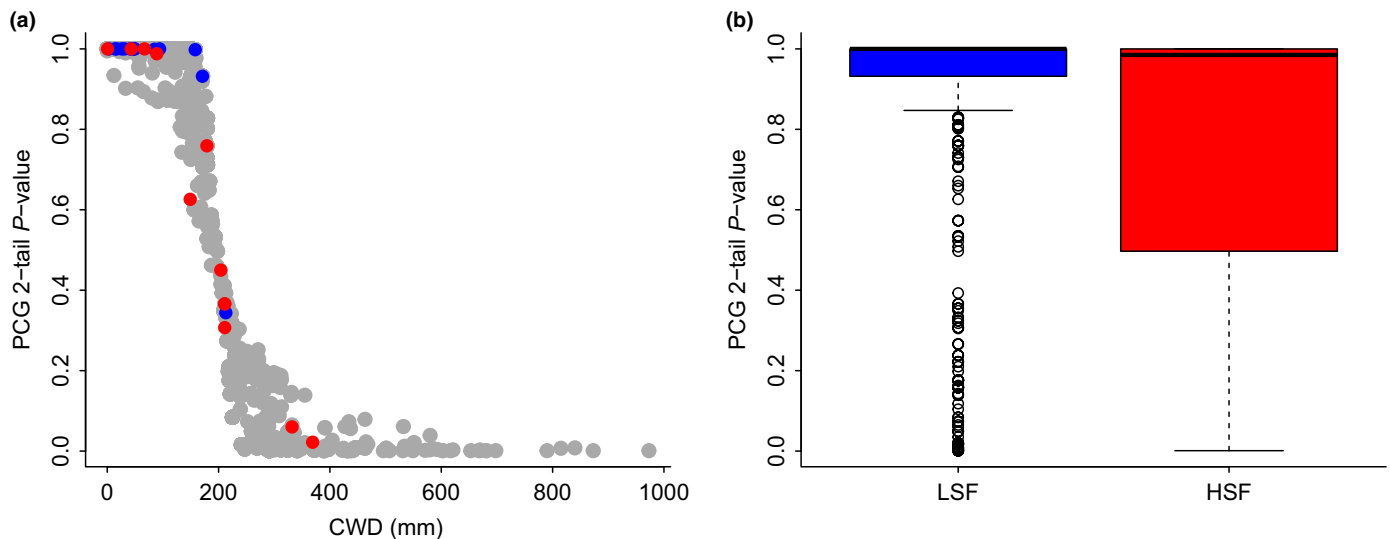


Fig. 4 (a) The probability of recording a higher dry-affiliated precipitation centre of gravity (PCG) value than observed by chance (PCG 2-tail P -value) for a range of genera in Amazonian sites varying with the Cumulative Water Deficit for the same sites obtained by Esquivel-Muelbert *et al.* (2017). Each point represents a different genus in the Amazon (grey points), where blue and red points represent the studied genera for LSF and HSF, respectively. (b) The PCG 2-tail P -value obtained from the database available at Esquivel-Muelbert *et al.* (2017) for all the genera recorded at LSF (blue) and HSF (red). The higher the genus PCG 2-tail P -value, the lower its dry affiliation index. We can see the lower dry affiliation of LSF genera (higher PCG 2-tail P -value, $P < 0.001$) when compared with the HSF genera. Whiskers in (b) are minimum value or, when outliers are present, 1.5 interquartile range below the quartile 2.

equally to VPD. Evapotranspiration (ET) was not affected by VPD_r neither was $CMWD_r$ ($P = 0.32$ and $P = 0.29$), although site had a significant effect on ET ($P < 0.001$) (Table S5; Fig. S4).

The differences in ecosystem canopy conductance (G_s) values between the two forests correlated with the variation observed in community Ψ_{min} , as represented by the dominance-weighted trait (Fig. 8). For the same G_s value, the HSF had more negative community Ψ_{min} than LSF, and the G_s seems to respond linearly to HSM_{P50} , which explained 95% of G_s variability, when the two sites were considered together ($P = 0.02$) (Fig. 8b).

Discussion

We evaluated plant responses at the species, community and ecosystem levels during typical years and one of the most severe drought events (El-Niño event in 2015) (Jiménez-Muñoz *et al.*, 2016) ever recorded in Amazonia. We report species-level hydraulic traits that contributed to the observed differences in forest drought responses. Our findings highlight the role of rainfall seasonality and interannual variability in precipitation as important filters selecting different hydraulic traits, strategies and taxa across rainforest sites, and complement analyses based on MAP differences alone (Choat *et al.*, 2012; Ciemer *et al.*, 2019). The dominant species at the high seasonality forest in the eastern Amazon (HSF) are more drought-affiliated and exhibit hydraulic traits with higher embolism resistance (i.e. lower P_{88}), as compared to the low seasonal forest in the central Amazon (LSF).

Despite this difference in the hydraulic system of the plants, both forests maintained the same sensitivity of canopy conductance (G_s) to atmospheric drought. Our data suggest this is possible because of the higher embolism resistance in HSF.

Interestingly, the two forests had similar responses to the 2015-ENSO when we consider their change in water potential, and at both forests we showed species embolism resistance modulated the species-level response to ENSO. Importantly, despite the limitations of our sampling design, we were able to show that species-level hydraulic traits have the potential of being scaled up to community-level properties, which in turn could help in explaining ecosystem-level water fluxes and drought response (Fig. 8).

Differences in drought resistance traits between low and high seasonality forests

Our results indicate that precipitation regime is an important filter in selecting contrasting embolism vulnerabilities. The drier condition and the marked seasonality and interannual rainfall variability in eastern Amazon make the HSF an environment with more pronounced water limitation, which in turn, has shaped the dominance of traits related to embolism resistance that allowed species to operate at more negative Ψ during water-limiting conditions. Consistent with these findings, our results indicate a higher proportion of dry-affiliated taxa at the HSF when compared with the LSF (Fig. 4) (Esquivel-Muelbert *et al.*, 2017), and the dominance of drought-resistant taxa in the HSF also suggests that climate-driven community assembly may be the mechanism underlying the higher resilience to climatic disturbances observed for forests under higher rainfall variability regimes in the Amazon (Ciemer *et al.*, 2019).

The differences between P_{88} and P_{50} show that xylem embolism resistance (represented by the vulnerability curve) can be affected not only by shifting the curves towards a certain P_{50} , but also by modifying their shape (i.e. the slope and the

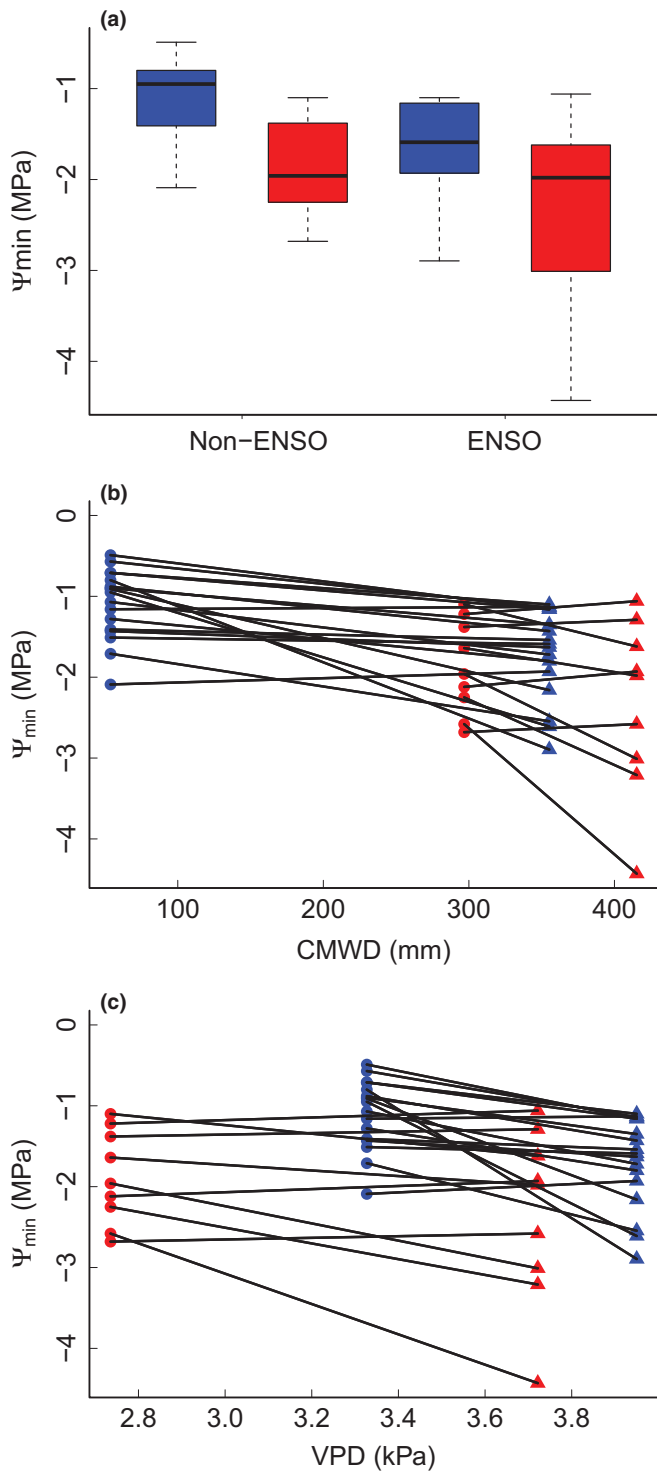


Fig. 5 (a) Dry season minimum leaf water potential (Ψ_{\min} ; MPa) of high seasonality forest (HSF; Tapajos) and the low seasonality forest (LSF; Manaus) species during non-ENSO year (blue) and the 2015-ENSO year (red). Change in minimum leaf water potential (Ψ_{\min} ; MPa) from non-ENSO (circles) to the 2015-ENSO year (triangles) in the low seasonality forest (LSF, Manaus; blue) and the high seasonality forest (HSF, Tapajos, red) as a function of monthly CMWD, and (b) maximum monthly vapour pressure deficit (VPD); (c) Each pair of points (circle and triangle) represents a different species.

difference between P_{50} and P_{88}) (Fig. 2). We observed a lower P_{88} in the HSF, which could be an evolutionary adjustment allowing these species to maintain xylem conductivity in highly seasonal environments where some embolism may be unavoidable, mainly for shallow-rooted species in HSF (Brum *et al.*, 2018). Thus, we emphasize the importance of xylem embolism resistance (represented by the vulnerability curves) as one of key functional traits relevant for explaining the patterns of plant distribution in biodiverse tropical ecosystems, as proposed for other environments (Pockman & Sperry, 2000; Brodrribb, 2017; Cosme *et al.*, 2017; Trueba *et al.*, 2017; Oliveira *et al.*, 2019).

Complex leaf water potential response to the 2015-ENSO-induced drought

During the 2015-ENSO, the Amazon Basin-wide average temperature reached a record high (annual monthly maximum was 2.5°C higher than the climatological mean) for the last century, exacerbating the effect of the 2015-ENSO drought (Jiménez-Muñoz *et al.*, 2016; Panisset *et al.*, 2018). The warmer conditions increased the evaporative demand (VPD) at both sites, affecting species hydraulic functioning. Our results showed a site-specific condition affecting Ψ_{\min} (Fig. 5), with the CMWD likely incor-

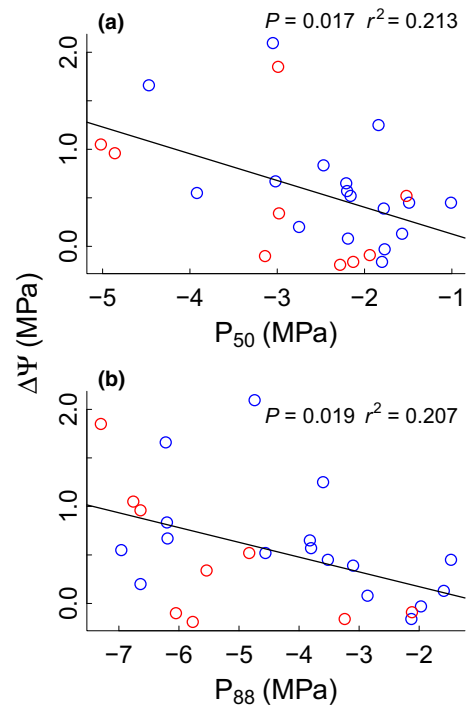


Fig. 6 Relationship between change in minimum leaf water potential from non-ENSO year to 2015-ENSO year ($\Delta\Psi$; MPa) and embolism resistance for the low seasonality forest (LSF, Manaus, blue) and the high seasonality forest (HSF, Tapajos, red). Relationship between $\Delta\Psi$ and (a) P_{50} and (b) P_{88} . The solid lines represent the best linear fit. Whiskers in (a) are either maximum/minimum value or, when outliers are present, 1.5 interquartile range above/below the quartiles 2 and 3.

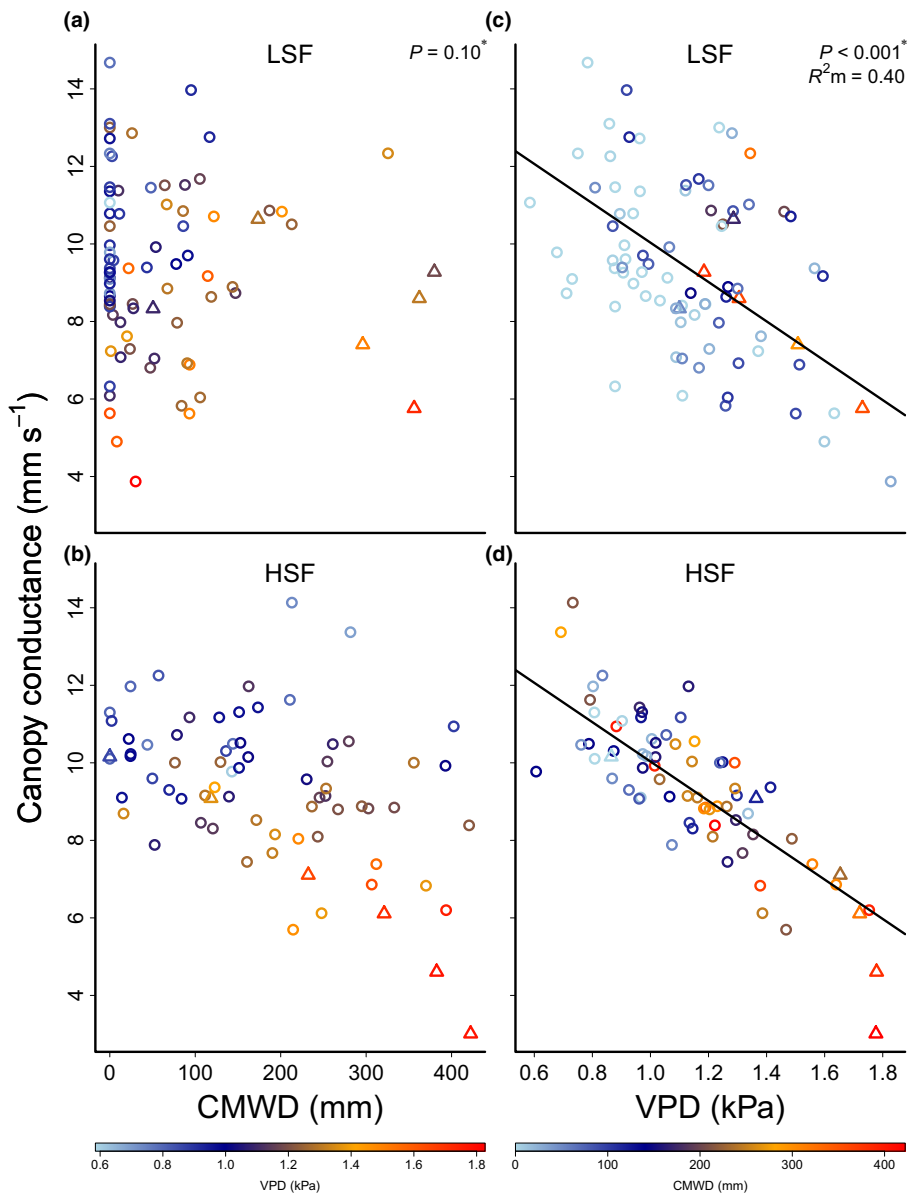


Fig. 7 Relationship between July to December monthly mean canopy conductance (G_s) and cumulative water deficit (CMWD) in (a) low seasonality forest (LSF, Manaus) and (b) high seasonality forest (HSF, Tapajos), and between canopy conductance (G_s) and monthly mean vapour pressure deficit (VPD) for (c) LSF and (d) HSF. The colour of the data points is proportional to the VPD value in plots (a) and (b) and to the CMWD values in plots (c) and (d), according to the colour charts below the panels. Note that high CMWD data points are redder, indicating they also have high VPD showing the correlation between VPD and CMWD. The P -values* are for the relationship between G_s and VPD_r and CMWD_r, which are the same variables after removing the correlation between VPD and CMWD using residuals (see the Data analysis subsection and the Results). Note both sites were modelled together and the P -value in panel (a) also applies to (b), and P and R^2 values in (c) also apply to (d). Triangle points are data from 2015-ENSO. Circle points are monthly data from 1999 to 2016, excluding the 2015-ENSO period. Another version of this figure presenting the G_s relationship to VPD_r and CMWD_r, is presented in Supporting Information Fig. S3.

porating both the atmospheric signal (VPD) and the soil signal (CMWD) in plant water potential.

This difficulty in separating soil and atmospheric water stress, as both usually occur together, is furthermore complicated by the non-linear effect of soil water content (represented in our study sites by the CMWD) on soil water potential (van Genuchten, 1980), which means it is necessary to have substantial decrease in CMWD for the soil water potential to increase to levels that induce embolism; and once this threshold is reached a small change in CMWD implies a large change in soil water potential. This threshold has an important consequence for vegetation, as it represents the point when plants start experiencing a strong soil drought signal, which depends on: (1) soil type and soil depth, (2) tree rooting depth, and (3) spatial variability, all factors that can imply landscape niches with different degrees of vulnerability. So, depending on the locations and species, the CMWD can

have different meanings, and should be used with caution as universal index of drought stress for vegetation (Esquivel-Muelbert *et al.*, 2017). For example, the higher drop in Ψ observed for some species at the HSF could indicate the placement of their roots in shallow soils and less stomatal regulation, while deep-rooted species probably avoid extreme intensity of droughts (e.g. Nepstad *et al.*, 1994; Oliveira *et al.*, 2005; Ivanov *et al.*, 2012; Brum *et al.*, 2018).

Although we observed a strong climatological drought, we cannot predict its consequences for long-term functioning of trees, as it does not immediately translate to ecohydrological drought (Nepstad *et al.*, 2007; Da Costa *et al.*, 2010) and some species were still operating within some hydraulic safety margin. We found the drought was enough to cause a modest average drop in leaf Ψ (with Ψ stabilization), probably indicating species stomatal control, with the major effect at gas exchange level, as observed

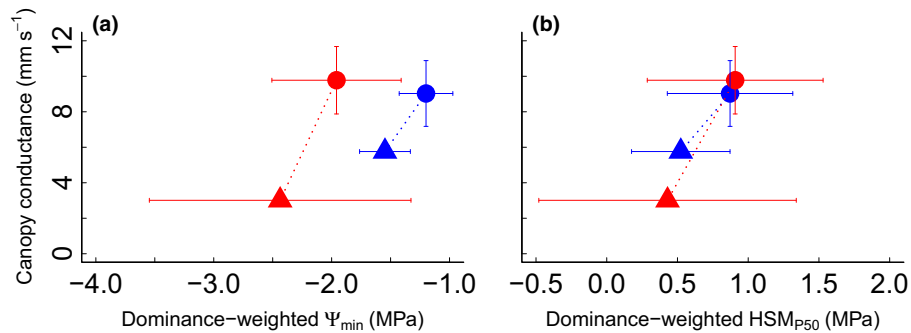


Fig. 8 Canopy conductance (mm s^{-1}) in non-ENSO (circles) and ENSO (triangles) years and for LSF (blue) and HSF (red) vs: (a) the dominance-weighted minimum leaf water potential (Ψ_{min} ; MPa), and (b) P_{50} hydraulic safety margin (HSM_{P50} ; MPa). The horizontal bars represent the confidence interval (*ci*) for the dominance-weighted mean of Ψ_{min} and HSM. The vertical bars represent the SD, across typical years, of canopy conductance in August and December for LSF and HSF, respectively. We considered as typical (non-ENSO) years the period from 1999 to 2016, excluding data from 2015-ENSO. As ENSO year, we considered October and December of 2015 for LSF and HSF, respectively, and hence we had no monthly SD.

with the decrease in G_s , which is likely maintaining ET constant despite changing VPD, as predicted by stomatal optimization models (Sperry & Love, 2015; Eller *et al.*, 2018). We also show that xylem embolism resistance explained part of the response in leaf Ψ during the 2015-ENSO (Fig. 6), which means species with higher resistance to xylem embolism could withstand lower water potentials and maintain gas exchange under drier conditions. Thus, to obtain a more comprehensive understanding on the diversity of plant water potential responses, studies should consider traits that influence plant water supply, demand and storage, some of which are very challenging to measure in the field.

Canopy conductance changes as an ecosystem-level response

It is notable that, despite the HSF and LSF operating at different Ψ_{min} , both had the same canopy-level response to VPD (Fig. 7). This difference between water supply function responses with no difference in the canopy-level water control function responses is likely possible only because the HSF has a more embolism-resistant water transport system. This is theoretically expected, as the embolism resistance sets the water potentials under which plants can operate (Sperry & Love, 2015) and, consequently, modulate the atmospheric and soil climatic envelope they can tolerate.

In fact, we show here the Ψ_{min} and HSM are traits mechanistically involved in species physiological responses under different conditions of water availability (Fig. 8). Moreover, the result that both communities operate under the same safety margin, in ENSO and non-ENSO, suggests they can retain their gas exchange rates even under extreme drier conditions than the usual dry season, which probably directly influences forest productivity. This highlights the role of xylem embolism resistance traits in determining plant functioning and vegetation drought response (Anderegg *et al.*, 2016, 2018). Actually, including embolism resistance in plant models has improved the prediction of ecosystem transpiration drought responses in the Amazon forest of Caxiuana (Eller *et al.*, 2018), and such models also predict lower sensitivity to drought than previous models, a result supported by our data.

Despite changes in the CMWD we did not detect its signal in canopy-level response. In LSF, the effect of 2015-ENSO was only substantial in the superficial soil layers (*c.* 80 cm depth), suggesting that a higher CMWD (than that caused by the 2015-ENSO) is necessary to affect deeper soils and change the soil water content in a way that would induce notable changes in canopy conductance. On the other hand, in the HSF, the large variability in soil water content (at least to a depth of 2 m; Fig. S2) did not affect G_s either, emphasizing the importance of more drought-resistant traits and/or deeper roots to modulate canopy water use. This suggests possibly extreme dry years, and not average years, contribute to filter plant communities, where trees have adapted their water transport system to drier than normal conditions, which they will likely experience during their lifespan (Grant *et al.*, 2017). Moreover, as in HSF trees are currently operating at lower soil water availability, we believe that an additional increase in CMWD may provoke extreme changes in soil water potential (Hutyra *et al.*, 2005) and consequently in forest functioning. Additional studies will need to consider interactions between rooting depth and soil moisture dynamics to gain insights into the behaviour of forest canopy conductance.

Conclusion

We report significant differences in hydraulic traits between two Amazon forests: low (LSF) and high (HSF) seasonal forest. Our results demonstrate that the seasonal and interannual variability in water stress is a key factor driving hydraulic functional differences across tropical forest sites. Interestingly, despite differences in water transport operation and traits, this difference was not translated into different atmospheric drought responses, suggesting the more drought-resistant hydraulic traits in HSF compensated for the drier soils, equalizing their safety margin and allowing them to maintain similar canopy-level responses to a drier atmosphere in both forests.

Our study shows the importance of embolism resistance in explaining interspecific variability in drought responses of the two different communities of species that have contrasting

seasonality of moisture availability, thereby linking relevant traits to species distribution, community assembly and ecosystem functioning. Further studies should address how spatial and temporal climatic variability at broader scales in the Amazon region filter a set of hydraulic traits that affect forest functioning, which will permit better-informed predictions of vegetation response to climate change.







Acknowledgements

We acknowledge funding from Brazil-USA Collaborative Research GoAmazon (DE-FOA-0000919, FAPESP-2013/50531-2, FAPESP-2013/50533-5), Microsoft/FAPESP-2011/52072-0, US DOE nos. DE-SC0008383 and DE-SC0011078. NSF#1622721 supported NRC and K67 eddy-flux data. We thank CAPES for support of the scholarships of FdVB, PRB, MB, and other co-authors, and CNPq for RSO's productivity scholarship. VI acknowledges support from Google Inc. towards the project 'Evapotranspiration of the Green Ocean Amazon'. We thank the Newton International Fellowship (NF170370) who recently funded PRLB. We thank the Large-Scale Biosphere-Atmosphere (LBA) Program and Empresa Brasileira de Pesquisa Agropecuária (EMBRAPA, Santarem) for technical support. We thank Mr Kleber Campos and Dr Kenia Wiedemann for their support.

Author contributions

FdVB, PRLB, MB and RSO conceived the research ideas, developed the project and wrote the manuscript. FVB, PRLB and MB collected, processed and analysed the data. N-RC and SRS, with support from PG, derived the ecosystem analysis, principally metrics of whole forest water cycling (canopy conductance and cumulative water deficit) from eddy covariance data, after applying consistent processing and QA/QC protocols at both sites. LSB and BOC collected and processed soil data. DP, LP and GST collected and processed some tree hydraulic data. LFA, AJNL and VMCC collected, processed and analysed floristic data. LSML and ACA maintained instruments and acquired and processed raw eddy covariance data from the low-seasonality forest (K34), and SRS and NR-C played this role at the HSF (K67). LOECA, J-EL and VI and all authors revised the manuscript. FdVB, PRLB and MB contributed equally to this work.

ORCID

Luciana F. Alves  <https://orcid.org/0000-0002-8944-1851>
 Fernanda de V. Barros  <https://orcid.org/0000-0003-3835-2020>
 Bradley O. Christoffersen  <https://orcid.org/0000-0002-4890-9999>
 Rafael S. Oliveira  <https://orcid.org/0000-0002-6392-2526>
 Luciano Pereira  <https://orcid.org/0000-0003-2225-2957>
 Grazielle S. Teodoro  <https://orcid.org/0000-0002-5528-8828>

References

- Anderegg WRL, Flint A, Huang C, Flint L, Berry JA, Davis FW, Sperry JS, Field CB. 2015. Tree mortality predicted from drought-induced vascular damage. *Nature Geoscience* 8: 367–371.
- Anderegg WR, Klein T, Bartlett M, Sack L, Pellegrini AF, Choat B, Jansen S. 2016. Meta-analysis reveals that hydraulic traits explain cross-species patterns of drought-induced tree mortality across the globe. *Proceedings of the National Academy of Sciences, USA* 113: 5024–5029.
- Anderegg WRL, Konings AG, Trugman AT, Yu K, Bowling DR, Gabbitas R, Karp DS, Pacala S, Sperry JS, Sulman BN *et al.* 2018. Hydraulic diversity of forests regulates ecosystem resilience during drought. *Nature* 561: 538–541.
- Aragão LEOC, Malhi Y, Roman-Cuesta RM, Saatchi S, Anderson LO, Shimabukuro YE. 2007. Spatial patterns and fire response of recent Amazonian droughts. *Geophysical Research Letters* 34: L07701.
- Araujo AC, Nobre AD, Kruijt B, Elbers JA, Dallarosa R, Stefani P, von Randow C, Manzi O, Manzi AO, Culf AD *et al.* 2002. Comparative measurements of carbon dioxide fluxes from two nearby towers in a central Amazonian rainforest: the Manaus LBA site. *Journal of Geophysical Research* 107: 8090.
- Brienen RJW, Phillips OL, Feldpausch TR, Gloor E, Baker TR, Lloyd J, Lopez-Gonzalez G, Monteagudo-Mendoza A, Malhi Y, Martinez RA *et al.* 2015. Long-term decline of the Amazon carbon sink. *Nature* 519: 344–348.
- Brodribb TJ. 2017. Progressing from “functional” to mechanistic traits. *New Phytologist* 215: 9–11.
- Brum M, Vadeboncoeur MA, Ivanov V, Asbjornsen H, Saleska S, Alves LF, Penha D, Dias JD, Aragão LEOC, Barros F *et al.* 2018. Hydrological niche segregation defines forest structure and drought tolerance strategies in a seasonal Amazon forest. *Journal of Ecology* 107: 318–333.
- Carneiro VMC. 2004. *Composição florística e análise estrutural da floresta primária de terra firme na bacia do Rio Cuieras, Manaus – AM*. Masters Thesis, Universidade Federal do Amazonas, Manaus – AM, Brazil.
- Choat B, Jansen S, Brodribb TJ, Cochard H, Delzon S, Bhaskar R, Bucci GS, Field TS, Gleason SM, Hacke UG *et al.* 2012. Global convergence in the vulnerability of forests to drought. *Nature* 491: 752–755.
- Cierner C, Boers N, Hirota M, Kurths J, Muller-Hansen F, Oliveira RS, Winkelmann R. 2019. Higher resilience to climatic disturbances in tropical vegetation exposed to more variable rainfall. *Nature Geoscience* 12: 174–179.
- Collatz GJ, Ball JT, Grivet C, Berry JA. 1991. Physiological and environmental regulation of stomatal conductance, photosynthesis and transpiration: a model that includes a laminar boundary layer. *Agricultural and Forest Meteorology* 54: 107–136.
- Cosme LHM, Schiatti J, Costa FRC, Oliveira RS. 2017. The importance of hydraulic architecture to the distribution patterns of trees in a central Amazonian forest. *New Phytologist* 215: 113–125.
- Cox PM, Betts RA, Collins M, Harris PP, Huntingford C, Jones CD. 2004. Amazonian forest dieback under climate-carbon cycle projections for the 21st century. *Theoretical and Applied Climatology* 78: 137–156.
- Cox PM, Pearson D, Booth BB, Friedlingstein P, Huntingford C, Jones CD, Luke CM. 2013. Sensitivity of tropical carbon to climate change constrained by carbon dioxide variability. *Nature* 494: 341–344.
- Da Costa CL, Galbraith D, Almeida S, Tanaka Portela BT, da Costa M, de Athaydes SJ, Braga AP, Gonçalves PHL, Oliveira AAR, Fisher R *et al.* 2010. Effect of seven years of experimental drought on the aboveground biomass storage of an eastern Amazonian rainforest. *New Phytologist* 187: 579–591.
- Davidson E, Lefebvre PA, Brando PM, Ray DM, Trumbore SE, Solorzano LA, Ferreira JN, Bustamante MMC, Nepstad DC. 2011. Carbon inputs and water uptake in deep soils of an eastern Amazon forest. *Forest Science* 57: 51–58.
- De Gonçalves LGG, Borak JS, Costa MH, Saleska SR, Baker I, Restrepo-Coupe N, Muza MN, Poulter B, Verbeeck H, Fisher JB *et al.* 2013. Overview of the large-scale biosphere-atmosphere experiment in Amazonia data model intercomparison project (LBA-DMIP). *Agricultural and Forest Meteorology* 182–183: 111–127.
- Eller CB, Rowland L, Oliveira RS, Bittencourt PRL, Barros FV, Friend AD, Mencuccini M, Sitch S, Cox P. 2018. Modelling tropical forest responses to drought and El Niño with a stomatal optimization model based on xylem

- hydraulics. *Philosophical Transactions of the Royal Society of London. Series B: Biological Sciences* 373: 20170315.
- Engelbrecht BMJ, Comita LS, Condit R, Kursar TA, Tyree MT, Turner BL, Hubbell SP. 2007. Drought sensitivity shapes species distribution patterns in tropical forests. *Nature* 447: 80–82.
- Engelbrecht BMJ, Kursar TA, Tyree MT. 2005. Drought effects on seedling survival in a tropical moist forest. *Trees* 19: 312–321.
- Esquivel-Muelbert A, Baker TR, Dexter KG, Lewis SL, Brienen RJW, Feldpausch TR, Loyd J, Monteagudo-Mendoza A, Arroyo L, Álvarez-Dávila E, et al. 2018. Compositional response of Amazon forests to climate change. *Global Change Biology* 25: 39–56.
- Esquivel-Muelbert A, Baker TR, Dexter KG, Lewis SL, ter Steege H, Lopez-Gonzalez G, Mendoza AB, Brienen R, Feldpausch TR, Pitman N et al. 2017. Seasonal drought limits tree species across the Neotropics. *Ecography* 40: 618–629.
- Fauset S, Johnson MO, Gloor M, Baker TR, Monteagudo A, Brienen RJW, Feldpausch TR, Lopez-Gonzalez G, Malhi Y, ter Steege H et al. 2015. Species contributions to stems, biomass and productivity in Amazon inventory plots. Hyperdominance in Amazonian forest carbon cycling. *Nature Communications* 6: 6857.
- Fisher RA, Muszala S, Verstein M, Lawrence P, Xu C, McDowell NG, Knox RG, Koven C, Holm J, Rogers BM et al. 2015. Taking off the training wheels: the properties of a dynamic vegetation model without climate envelopes, CLM4.5(ED). *Geoscientific Model Development* 8: 3593–3619.
- Friedlingstein P, Cox P, Betts R, Bopp L, von Bloh W, Brovkin V, Cadulee P, Doneyf S, Eby M, Fungh I et al. 2006. Climate–carbon cycle feedback analysis: results from the (CMIP)-M-4 model intercomparison. *Journal of Climate* 19: 3337–3353.
- Fu R, Yin L, Li W, Arias PA, Dickinson RE, Huang L, Chakraborty S, Fernandes K, Liebmann B, Fisher R et al. 2013. Increased dry-season length over southern Amazonia in recent decades and its implication for future climate projection. *Proceedings of the National Academy of Sciences, USA* 110: 18110–18115.
- Garnier E, Cortez J, Billès G, Navas ML, Roumet C, Debussche M, Gérard L, Blanchard A, Aubry D, Neill C et al. 2004. Plant functional markers capture ecosystem properties during secondary succession. *Ecology* 85: 2630–2637.
- Gentine P, Guérin M, Uriarte M, McDowell NG, Pockman WT. 2016. An allometry-based model of the survival strategies of hydraulic failure and carbon starvation. *Ecophysiology* 9: 529–546.
- van Genuchten MT. 1980. A closed-form equation for predicting the hydraulic conductivity of unsaturated soils. *Soil Science Society of America Journal* 44: 892–898.
- Good P, Jones C, Lowe J, Betts R, Booth B. 2011. Quantifying environmental drivers of future tropical forest extent. *Journal of Climate* 24: 1337–1349.
- Grant PR, Grant BR, Huey RB, Johnson MTJ, Knoll AH, Schmitt J. 2017. Evolution caused by extreme events. *Philosophical Transactions of the Royal Society of London. Series B: Biological Sciences* 372: 20160146.
- Huntingford C, Zelazowski P, Galbraith D, Mercado LM, Sitch S, Fisher R, Lomas M, Walker AP, Jones CD, Booth BBB et al. 2013. Simulated resilience of tropical rainforests to CO₂-induced climate change. *Nature Geoscience* 6: 268–273.
- Hutyra LR, Munger JW, Nobre CA, Saleska SR, Vieira SA, Wofsy SC. 2005. Climatic variability and vegetation vulnerability in Amazonia. *Geophysical Research Letters* 32: L24712.
- Ivanov VY, Hutyra LR, Wofsy SC, Munger JW, Saleska SR, Oliveira RC Jr, Canavog PB. 2012. Root niche separation can explain avoidance of seasonal drought stress and vulnerability of overstory trees to extended drought in a mature Amazonian forest. *Water Resources Research* 48: W12507.
- Jiménez-Muñoz JC, Mattar C, Barichivich J, Santamaría-Artigas A, Takahashi K, Malhi Y, Sobrino JA, van der Schrier G. 2016. Record-breaking warming and extreme drought in the Amazon rainforest during the course of El Niño 2015–2016. *Scientific Reports* 6: 33130.
- Joezter E, Delire C, Douville H, Ciais P, Decharme B, Fisher R, Christoffersen B, Calvet JC, da Costa ACL, Ferreira L et al. 2014. Predicting the response of the Amazon rainforest to persistent drought conditions under current and future climates: a major challenge for global land surface models. *Geoscientific Model Development* 7: 2933–2950.
- Konings AG, Williams AP, Gentine P. 2017. Sensitivity of grassland productivity to aridity controlled by stomatal and xylem regulation. *Nature Geoscience* 7: 2193–2197.
- Levine NM, Zhang K, Longo M, Baccini A, Phillips OL, Lewis SL, Alvarez-Dávila E, Andrade ACG, Brienen RJW, Erwin TL et al. 2016. Ecosystem heterogeneity determines the ecological resilience of the Amazon to climate change. *Proceedings of the National Academy of Sciences, USA* 113: 793–797.
- Lin YS, Medlyn BE, Duursma RA, Prentice IC, Wang H, Baig S, Eamus D, Dios VR, Mitchell P, Ellsworth DS et al. 2015. Optimal stomatal behavior around the world. *Nature Climate Change* 5: 459–464.
- Lintner BR, Biasutti M, Diffenbaugh NS, Lee J-E, Niznik MJ, Findell KL. 2012. Amplification of wet and dry month occurrence over tropical land regions in response to global warming. *Journal of Geophysical Research* 117: D11106.
- Longo M. 2013. *Amazon forest response to changes in rainfall regime: results from an individual-based dynamic vegetation model*. PhD Thesis: Harvard University, Cambridge, MA, USA.
- Malhi Y, Aragão LE, Galbraith D, Huntingford C, Fisher R, Zelazowski P, Sitch S, McSweeney C, Meir P. 2009. Exploring the likelihood and mechanism of a climate-change-induced dieback of the Amazon rainforest. *Proceedings of the National Academy of Sciences, USA* 106: 20610–20615.
- Manoli G, Ivanov VY, Fatichi S. 2018. Dry-season greening and water stress in Amazonia: the role of modeling leaf phenology. *Journal of Geophysical Research* 123: 1909–1926.
- Markesteyn L, Poorter L, Bongers F, Paz H, Sack L. 2011. Hydraulics and life history of tropical dry forest tree species: coordination of species' drought and shade tolerance. *New Phytologist* 191: 480–495.
- McDowell N, Pockman WT, Allen CD, Breshears DD, Cobb N, Kolb T, Plaut J, Sperry J, West A, Williams DG et al. 2008. Mechanisms of plant survival and mortality during drought: Why do some plants survive while others succumb to drought? *New Phytologist* 178: 719–739.
- Medlyn BE, De Kauwe MG, Duursma RA. 2016. New developments in the effort to model ecosystems under water stress. *New Phytologist* 212: 5–7.
- Meinzer FC, Johnson DM, Lachenbruch B, McCulloh KA, Woodruff DR. 2009. Xylem hydraulic safety margins in woody plants: coordination of stomatal control of xylem tension with hydraulic capacitance. *Functional Ecology* 23: 922–930.
- Nepstad DC, de Carvalho CR, Davidson EA, Jipp PH, Lefebvre PA, Negreiros GH, Silva ED, Stone TA, Trumbore SE, Vieira S. 1994. The role of deep roots in the hydrological and carbon cycles of Amazonian forests and pastures. *Nature* 372: 666–669.
- Nepstad DC, Tohver IM, Ray D, Moutinho P, Cardinot G. 2007. Mortality of large trees and lianas following experimental drought in an Amazon Forest. *Ecology* 88: 2259–2269.
- Oliveira RS, Costa FRC, Baalen E, Jonge A, Bittencourt PR, Almanza Y, Barros FV, Cordoba EC, Fagundes MV, Garcia S et al. 2019. Embolism resistance drives the distribution of Amazonian rainforest tree species along hydro-topographic gradients. *New Phytologist* 221: 1457–1465.
- Oliveira RS, Dawson TE, Burgess SSO, Nepstad DC. 2005. Hydraulic redistribution in three Amazonian trees. *Oecologia* 145: 354–363.
- Oyama MD, Nobre CA. 2003. A new climate–vegetation equilibrium state for Tropical South America. *Geophysical Research Letters* 30: 2199.
- Pammenter NW, Vander Willigen C. 1998. A mathematical and statistical analysis of the curves illustrating vulnerability of xylem to cavitation. *Tree Physiology* 18: 589–593.
- Panisset JS, Libonati R, Gouveia CMP, Machado-Silva F, França DA, França JRA, Peres LF. 2018. Contrasting patterns of the extreme drought episodes of 2005, 2010 and 2015 in the Amazon Basin. *International Journal of Climatology* 38: 1096–1104.
- Parrotta JA, Francis JK, DeAlmeida RR. 1995. *Trees of the Tapajós: A photographic field guide*. Gen. Tech. Rep. IITF-1, US Department of Agriculture, Rio Piedras, Puerto Rico.
- Pereira L, Bittencourt PRL, Oliveira RS, Junior MBM, Barros FV, Ribeiro RV, Mazzafra P. 2016. Plant pneumatics: stem air flow is related to embolism – new perspectives on methods in plant hydraulics. *New Phytologist* 211: 357–370.
- Phillips OL, van der Heijden G, Lewis SL, López-González G, Aragão LEOC, Lloyd J, Malhi Y, Monteagudo A, Almeida S, Dávila EA et al. 2010. Drought mortality relationships for tropical forests. *New Phytologist* 187: 631–646.

- Pockman WT, Sperry JS. 2000. Vulnerability to xylem cavitations and the distribution of Sonoran Desert vegetation. *American Journal of Botany* 87: 1287–1299.
- Pyle EH, Santoni GW, Nascimento HEM, Hutrya LR, Vieira S, Curran DJ, van Haren J, Saleska SR, Chow VY, Camargo PB. 2008. Dynamics of carbon, biomass, and structure in two Amazonian forests. *Journal of Geophysical Research: Biogeosciences* 114: 1–20.
- R Core Team. 2018. *R: a language and environment for statistical computing, v.3.5*. Vienna, Austria: R Foundation for Statistical Computing. [WWW document] URL <https://www.R-project.org/>
- Restrepo-Coupe N, Levine NM, Christoffersen BO, Albert LP, Wu J, Costa MH, Galbraith D, Imbuzeiro H, Martins G, Araujo AC *et al.* 2016. Do dynamic global vegetation models capture the seasonality of carbon fluxes in the Amazon basin? A data-model intercomparison. *Global Change Biology* 23: 191–208.
- Rowland L, da Costa ACL, Galbraith DR, Oliveira RS, Binks OJ, Oliveira AAR, Pullen AM, Doughty CE, Metcalfe DB, Vasconcelos SS *et al.* 2015. Death from drought in tropical forests is triggered by hydraulics not carbon starvation. *Nature* 528: 119–122.
- Sakschewski B, von Bloh W, Boit A, Poorter L, Peña-Claros M, Heinke J, Joshi J, Thonicke K. 2016. Resilience of Amazon forests emerges from plant trait diversity. *Nature Climate Change* 6: 1032–1036.
- Schneider CA, Rasband WS, Eliceiri KW. 2012. NIH Image to ImageJ: 25 years of image analysis. *Nature Methods* 9: 671–675.
- Scholz A, Klepsch M, Karimi Z, Jansen S. 2013. How to quantify conduits in wood? *Frontiers in Plant Science* 4: 56.
- Sperry JS, Donnelly JR, Tyree MT. 1988. A method for measuring hydraulic conductivity and embolism in xylem. *Plant, Cell & Environment* 11: 35–40.
- Sperry JS, Hacke UG, Oren R, Comstock JP. 2002. Water deficits and hydraulic limits to leaf water supply. *Plant, Cell & Environment* 25: 251–263.
- Sperry JS, Love DM. 2015. What plant hydraulics can tell us about responses to climate-change droughts. *New Phytologist* 207: 14–27.
- Ter Steege H, Pitman NCA, Sabatier D, Baraloto C, Salomao RP, Guevara JE, Phillips OL, Castillo CV, Magnusson WE, Molino JF *et al.* 2013. Hyperdominance in the Amazonian Tree Flora. *Science* 342: 1243092.
- Trueba S, Pouteau R, Lens F, Feild TS, Isnard S, Olson ME, Delzon S. 2017. Vulnerability to xylem embolism as a major correlate of the environmental distribution of rain forest species on a tropical island. *Plant, Cell & Environment* 40: 277–289.
- Tyree MT, Sperry JS. 1989. Vulnerability of xylem to cavitation and embolism. *Annual Review of Plant Physiology and Plant Molecular Biology* 40: 19–38.
- Vieira S, de Camargo PB, Selhorst D, da Silva R, Hutrya L, Chambers JQ, Brown IF, Higuchi N, dos Santos J, Wofsy SC *et al.* 2004. Forest structure and carbon dynamics in Amazonian tropical rain forests. *Oecologia* 140: 468–479.
- Williamson GB, Laurance WF, Oliveira AA, Delamônica P, Gascon C, Lovejoy TE, Pohl L. 2000. Amazonian tree mortality during the 1997 El Niño drought. *Conservation Biology* 14: 1538–1542.
- Xu X, Medvigy D, Powers JS, Becknell JM, Guan K. 2016. Diversity in plant hydraulic traits explains seasonal and inter-annual variations of vegetation dynamics in seasonally dry tropical forests. *New Phytologist* 212: 80–95.

Supporting Information

Additional Supporting Information may be found online in the Supporting Information section at the end of the article.

Fig. S1 Times series of climatic and hydrologic variables for the studied sites.

Fig. S2 Soil water content time series for the studied sites.

Fig. S3 Relationship between monthly mean canopy conductance and residuals of vapour pressure deficit and cumulative water deficit for the studied sites.

Fig. S4 The relationship between monthly mean evapotranspiration and vapour pressure deficit and cumulative water deficit for the studied sites.

Methods S1 Species dominance and trait distribution in the communities.

Methods S2 The biogeographic dry affiliation index as a trait to distinguish LSF and HSF community composition.

Methods S3 Eddy covariance flux measurements.

Methods S4 Canopy conductance calculation

Methods S5 Statistic functions and packages

Table S1 List of species names, family and mean hydraulic trait values for all studied species at low seasonal forest (LSF) and high seasonal forest (HSF).

Table S2 Summary of hydraulic traits and statistical results of hypothesis 1, that HSF has more drought-resistant hydraulic traits than LSF.

Table S3 General mixed model result from the test of hypothesis 2, that species from HSF are less sensitive to ENSO than species from LSF.

Table S4 General mixed model result from the test of our hypothesis 3, that HSF is less sensitive to atmospheric drought and soil drought than the LSF.

Table S5 General mixed site-specific model results for evapotranspiration (ET) varying in function of atmospheric drought and soil drought.

Please note: Wiley Blackwell are not responsible for the content or functionality of any Supporting Information supplied by the authors. Any queries (other than missing material) should be directed to the *New Phytologist* Central Office.